Research Article

Mohammed Abdalbagi*

Micropolar flow and heat transfer within a permeable channel using the successive linearization method

https://doi.org/10.1515/phys-2023-0177
received September 30, 2023; accepted December 21, 2023

Abstract: This research investigates the flow of micropolar fluid and heat transfer through a permeable channel using the successive linearization method (SLM). The study considers parameters such as coupling, spin-gradient viscosity, and micro-inertia density. The partial differential equations involved are transformed into a system of ordinary differential equations using similarity variables. The resulting nonlinear equations are solved using the SLM technique, and their accuracy and computational efficiency are validated through comparative analysis with previous results. The study shows that increasing the parameters of coupling and spin-gradient viscosity has a positive impact on fluid flow, microrotation, heat transfer, and mass transport, as demonstrated by the increased dimensionless profiles. Conversely, an increase in the micro-inertia density parameter leads to a reduction in these profiles. This decrease can be attributed to the increase in the micro-inertia effect of fluid flow and heat transfer, resulting in a decrease in convection and a change in the flow pattern in the channel. Additionally, higher Reynolds numbers are associated with decreases in velocity, microrotation, temperature, and concentration distribution. This implies a reduction in fluid flow intensity, weaker heat transfer, and decreased mass transport. However, an increased Peclet number results in increased fluid temperature and concentration profiles, indicating enhanced thermal convection and mass transport. These findings have significant implications for applications involving micropolar fluids, such as lubrication systems, blood flow, microchannels, and filtration systems.

Keywords: micropolar fluids, heat and mass transfer, permeable channel, successive linearization method, Chebyshev spectral method

1 Introduction

The field of micropolar fluid mechanics, particularly in the study of non-Newtonian fluids, has made significant progress in recent years. A prominent figure in this progress is Eringen [1], whose pioneering contributions to the analysis of micropolar liquids have opened up new possibilities and approaches to understanding various phenomena. These phenomena include the dynamics of low-concentration suspensions, liquid crystals, blood flow, lubrication processes, and industrial applications.

Scientists and researchers have thoroughly used the micropolar theory to tackle several scientific and engineering problems. Heat transfer in micropolar boundary layer flow over a flat plate was investigated by Gorla *et al.* [2], who found that micropolar fluid characteristics had a major impact. Gorla [3] investigated the buoyancy effects on the flow and heat transfer of a micropolar fluid in a boundary layer flow along a vertical cylinder. In addition, Gorla [4] explored mixed convection in a micropolar fluid from a vertical surface with uniform heat flow, addressing the combined influences of forced and natural convection. Arafa and Gorla [5] studied the effects of buoyancy and curvature on convection along vertical cylinders and needles inserted in a micropolar fluid. They used a finite difference approach to numerically solve the governing equations for energy, momentum, and angular momentum. Raptis [6] examined the micropolar fluid flow through a porous medium using the generalized Darcy equation. Using the homotopy analysis method, Ziabakhsh and Domairry [7] could approximate micropolar flow in a porous channel with a high rate of mass transfer. Mohamed and Abo-Dahab [8] studied the combined effects of chemical reaction, thermal radiation, and heat generation on heat and mass transfer in

* **Corresponding author: Mohammed Abdalbagi**, Department of Science and Technology, Mathematics Program, Ranyah University College, Taif University, P.O. Box 11099, Taif, 21944, Saudi Arabia, e-mail: dr.m.bagi@gmail.com

magnetohydrodynamic (MHD) micropolar flow over a vertically moving porous plate in a porous medium.

Numerous scientists and researchers have examined the applications of micropolar fluids and nanofluids. A simulation of MHD biorheologic transport phenomena under blood flow control and filtration in porous medium was performed by Rashidi *et al.* [9]. They studied velocity and pressure profiles, along with their influence on magnetic field strength and the properties of porous media. Turkyilmazoglu [10] studied the behavior of micropolar fluids over a shrinking porous sheet, focusing on the flow and heat transfer characteristics. Prakash and Muthtamilselvan [11] explored the influence of radiation on the transient MHD flow of micropolar fluids between two porous vertical plates with boundary conditions of the third kind and discovered that thermal radiation reduced the temperature of the fluid. In a study conducted by Fakour *et al.* [12], they examined the behavior of flow and heat transfer, in a channel with permeable walls. Turkyilmazogl [13] explored the micropolar fluid flow due to a porous stretching sheet and heat transfer. According to Sheikholeslami *et al.* [14], magnetic fields play a crucial role in the unsteady flow and heat transfer of nanofluids. In a subsequent study [15], they investigated the free convection of magnetic nanofluids and observed that the viscosity of the MFD led to significant changes in flow patterns and heat transfer characteristics. Mirzaaghaian and Ganji [16] applied the differential transformation method to study the micropolar fluid flow and heat transfer through a channel with permeable walls. Doh *et al.* [17] studied the transient heat and mass transfer of a micropolar fluid in a porous vertical channel with boundary conditions of the third kind. They analyzed the temperature, velocity, and concentration profiles and the effects of various parameters on heat and mass transfer. Another study by Doh *et al.* [18] investigated how internal heat sources affect the flow behavior, velocity distribution, and temperature profiles of a micropolar fluid in a porous vertical channel. The effect of heat transfer on electrically conducting MHD micropolar fluid flow along a semi-infinite horizontal plate with radiation and heat source was examined by Mishra *et al.* [19]. In their work, the obtained governing equations were converted into a set of dimensionless differential equations and then numerically solved using the well-known Runge–Kutta (R–K) method with a shooting technique.

Pattnaik *et al.* [20] investigated the effects of velocity slip on MHD flow over a stretching surface and found that the presence of velocity slip has significant implications on flow and thermal characteristics. Simultaneously, Mishra *et al.* [21] studied nonlinear radiations and cross-diffusion effects on the convection of micropolar nanoliquids toward a stretching sheet with an exponential heat source, highlighting the significant effect of radiation and cross-diffusion parameters on streamline movement and heat transport. Saraswathy *et al.* [22] used sensitivity analysis to study the asymmetric flow and heat transfer in micropolar fluids, highlighting the crucial role played by Arrhenius energy in characterizing these flows. A theoretical study on non-Newtonian micropolar nanofluid flow by Nadeem *et al.* [23] emphasized the impact of non-Newtonian behavioral characteristics and nanoparticle concentration on fluid flow and heat transfer processes. Furthermore, Abbas and Shatanawi [24] studied the heat and mass transfer in a Casson micropolar nanofluid over a stretchable Riga surface, where they highlighted the importance of stretching parameters and nanoparticle volume fraction on fluid and heat transport capabilities. The subject was advanced by Saraswathy *et al.* [25] through a theory on the bioconvection of micropolar fluid under consideration for the Cattaneo–Christov heat flux theorem. The combined effects of nonlinear thermal radiation, viscous dissipation, and magnetic field on MHD micropolar fluid flow in a porous channel were explored by Saraswathy *et al.* [26]. In their work, the nonlinear governed equations were solved numerically using the R-K integration procedure with the shooting method and analytically using the variational iteration method and Adomian decomposition method. They found that viscous dissipation and non-linear thermal radiation significantly influence the fluid flow and heat transfer within the porous channel. Humane *et al.* [27] also investigated the role of thermal or solutal convection in the behavior of a magneto-micropolar fluid inside an inclined porous stretching device. Shamshuddin *et al.* [28] investigated how variations in the thermal Peclet number, vortex viscosity, and Reynolds number affect the two-dimensional flow of a micropolar fluid passing through a channel due to combined convection. Their findings revealed the impact of these parameters on fluid properties such as velocity and thermal profiles. In another study, Shamshuddin *et al.* [29] applied the Chebyshev spectral method to examine the flow of nanofluid across an extended flat surface in the presence of an angled magnetic field. They focused on the heat transfer characteristics and how the orientation of the magnetic field influenced the flow behavior. The influence of elastic distortion on the conduction of heat in a motor oil was investigated by Salawu *et al.* [30] using hybridized single-walled carbon nanotube-silver and multi-walled carbon nanotube-molybdenum tetrasulfide magneto-nanomaterials. They found that both hybrid nanofluids exhibited less heat transmission at increased elastic distortion.

The physical application of this research concerns flow in porous channels, as discussed in detail by Harwin [31]

and Jalili *et al.* [32]. Laminar flow through a channel with porous walls is an idealized representation of the flow behavior that occurs in relevant geometries in the real world. This physics can be applied to model various processes, such as transpiration cooling, in which a cooler liquid flows over the outside of a heated, liquid-containing pipe or channel to prevent the walls from overheating. Another application of this flow modeling is the production of nuclear reactor fuel through the gaseous emission of the uranium-235 and uranium-238 isotope separation process. In addition, it can be used to control fluid flow through or into an aircraft wing, or as part of a model for flow past a membrane or filter to regulate the boundary-layer flow over the wing.

When examining and analyzing the current literature on micropolar fluid flow and heat transfer within a permeable channel, it was found that the numerical simulation of the recommended flow field has not been specifically studied using the successive linearization method (SLM). The corresponding non-dimensional ordinary differential equations are obtained by applying similarity transformations to the governed partial differential equations, and then, SLM is used to numerically address them. The results of the SLM are then compared with previous solutions presented by Mirgolbabaee *et al.* [33], who used the Akbari–Ganji method (AGM).

The motivation for this study is to illustrate the present algorithm in solving a highly nonlinear system of ordinary differential equations that controls micropolar fluid flow and heat transfer within a permeable channel. Additionally, it aims to investigate the effects of Reynolds numbers, microrotation or angular velocity, and Peclet number on flow properties, heat transfer, and concentration profiles. This study provides detailed profiles of velocity, temperature, and concentration.

SLM has been applied to solve the governing coupled nonlinear system of equations in a limited number of studies [34–41]. However, Awad *et al.* [42] and Makukula *et al.* [43] have demonstrated that SLM has high accuracy and fast convergence to numerical solutions. Furthermore, by efficiently handling nonlinear boundary value problems, the SLM approach outperforms conventional numerical techniques such as R–K shooting, finite differences, and finite elements.

The following steps were followed in writing this manuscript: Section 2 develops the mathematical model of the relevant work, and Section 3 describes the proposed numerical method. The numerical results presented in the tables and graphs are explained in Section 4. Finally, the main conclusions of this study are presented in Section 5.

The research questions that contribute to the novelty of this study are as follows:

- Can SLM effectively solve the system of fourth-order nonlinear equations governing micropolar fluid flow and heat transfer within a permeable channel?
- How does the angular or microrotation velocity parameter affect the determined velocity, micro-rotation, temperature, and concentration profiles?
- How does the Reynolds number affect the dimensionless flow function, microrotation, temperature, and concentration profiles?
- What effects does the Peclet number for heat and mass transfer have on the temperature and concentration profiles?

2 Mathematical formulation

In this study, we studied the steady flow of a micropolar fluid in a two-dimensional channel with parallel porous walls. The channel has a uniform injection or removal of fluid at a constant speed, as represented by v_0. The lower wall of the channel has a solute concentration denoted by C_1 and temperature denoted by T_1, whereas the upper wall has a solute concentration C_2 and temperature T_2. The channel walls are aligned parallel to the x-axis and positioned at $y = \pm h$, indicating the channel width (as shown in Figure 1). The governing equations that describe this flow can be found in the study of Sibanda and Awad [44]:

$$\frac{\partial u}{\partial x} + \frac{\partial v}{\partial y} = 0, \tag{1}$$

$$\rho\left(u\frac{\partial u}{\partial x} + v\frac{\partial u}{\partial y}\right) = -\frac{\partial p}{\partial x} + (\mu + k)\left(\frac{\partial^2 u}{\partial x^2} + \frac{\partial^2 u}{\partial y^2}\right) + k\frac{\partial N}{\partial y}, \tag{2}$$

$$\rho\left(u\frac{\partial u}{\partial x} + v\frac{\partial u}{\partial y}\right) = -\frac{\partial p}{\partial y} + (\mu + k)\left(\frac{\partial^2 u}{\partial x^2} + \frac{\partial^2 u}{\partial y^2}\right) - k\frac{\partial N}{\partial x}, \tag{3}$$

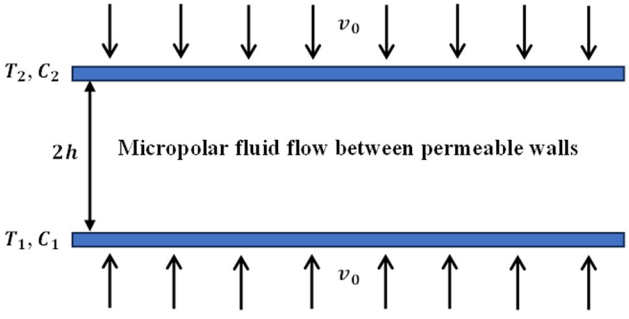

Figure 1: Schematic representation of the problem.

$$\rho\left(u\frac{\partial N}{\partial x}+v\frac{\partial N}{\partial y}\right)=-\frac{k}{j}+\left(2N+\frac{\partial u}{\partial x}-v\frac{\partial v}{\partial y}\right)+\frac{\mu_s}{j}\left(\frac{\partial^2 N}{\partial x^2}+\frac{\partial^2 N}{\partial y^2}\right), \tag{4}$$

$$\rho\left(u\frac{\partial T}{\partial x}+v\frac{\partial T}{\partial y}\right)=\frac{k_1}{C_p}\frac{\partial^2 T}{\partial y^2}, \tag{5}$$

$$\rho\left(u\frac{\partial C}{\partial x}+v\frac{\partial C}{\partial y}\right)=D^*\frac{\partial^2 C}{\partial y^2}. \tag{6}$$

In these equations, we have various variables and parameters. The velocity components are denoted by u and v along the x- and y-axes, respectively. Other variables include fluid density (ρ), dynamic viscosity (μ), angular or microrotation velocity (N), fluid pressure (p), fluid temperature (T), specific heat at constant pressure (C_p), species concentration (C), thermal conductivity (k_1), molecular diffusivity (D^*), micro-inertia density (j), and material parameter (k). The microrotation viscosity is represented by $\nu_s = (\mu + k/2)j$. The relevant boundary conditions for this scenario are as follows:

$$\left.\begin{aligned} y=-h:&\quad v=u=0,\quad N=-s\frac{\partial u}{\partial y},\\ y=+h:&\quad v=0,\quad u=\frac{v_0 x}{h},\quad N=\frac{v_0 x}{h^2}.\end{aligned}\right\} \tag{7}$$

In the context of the problem we are addressing, the boundary parameter s is used to indicate the rotational freedom of microelements near the walls of the channel. The value of s determines different scenarios. When $s = 0$, it represents concentrated particle flows where the microelements close to the wall cannot rotate. Other cases found in the literature include $s = 0.5$, which indicates the weak concentrations with the disappearance of the antisymmetric part of the stress tensor, and $s = 1$, which represents the turbulent flow. To simplify the equations governing this system, we introduce dimensionless variables as follows:

$$\eta=\frac{y}{h},\quad \psi=-v_0 x f(\eta),\quad N=\frac{v_0 x}{h^2}g(\eta),\quad \theta(\eta)=\frac{T-T_2}{T_1-T_2},\quad \text{and}\quad \phi(\eta)=\frac{C-C_2}{C_1-C2}, \tag{8}$$

where $T_2 = T_1 - Ax$ and $C_2 = C_1 - Bx$, with A and B being constants. The stream function is defined in the usual manner as follows:

$$u=\frac{\partial \psi}{\partial y},\quad \text{and}\quad v=-\frac{\partial \psi}{\partial x}. \tag{9}$$

Applying these transformations, the governing system of Eqs (1)–(7) is converted to a nonlinear system [44]:

$$(1+N_1)f^{iv}-N_1 g-\mathrm{Re}(ff'''-f'f'')=0, \tag{10}$$

$$N_2 g''+N_1(f''-2g)-N_3\mathrm{Re}(fg'-f'g)=0, \tag{11}$$

$$\theta''+\mathrm{Pe}_h(f'\theta-f\theta')=0, \tag{12}$$

$$\phi''+\mathrm{Pe}_m(f'\phi-f\phi')=0, \tag{13}$$

subject to the boundary conditions:

$$\left.\begin{aligned}\eta=-1: f=f'=g=0,&\quad \theta=\phi=1,\\ \eta=+1: f=\theta=\phi=0,&\quad f'=-1, g=1.\end{aligned}\right\} \tag{14}$$

Several primary parameters of interest in this problem are the buoyancy ratio N and the Peclet numbers Pe_h and Pe_m, Reynolds number Re, and Grashof number Gr. These parameters are defined as follows:

$$\left.\begin{aligned} &N_1=\frac{k}{\mu},\quad N_2=\frac{\nu_s}{\mu h^2},\\ &N_3=\frac{j}{h^2},\quad \mathrm{Re}=\frac{v_0}{\nu}h,\quad \mathrm{Pr}=\frac{\nu\rho C_p}{k_1},\\ &\mathrm{Sc}=\frac{\nu}{D^*},\quad \mathrm{Gr}=\frac{gB_T A h^4}{\nu^2},\\ &\mathrm{Pe}_h=\mathrm{PrRe},\quad \text{and}\quad \mathrm{Pe}_m=\mathrm{ScRe},\end{aligned}\right\} \tag{15}$$

where Pr represents the Prandtl number, Sc is the generalized Schmidt number, N_1 corresponds to the coupling parameter, N_2 is the spin-gradient viscosity parameter, and N_3 represents the micro-inertia density parameter. Furthermore, the local Nusselt and Sherwood numbers, denoted as Nu_x and Sh_x, respectively, can be defined as:

$$\mathrm{Nu}_x=\frac{q''_{y=-h}x}{(T_1-T_2)k_1}=-\theta'(-1),\quad \mathrm{Sh}_x=\frac{m''_{y=-h}x}{(C_1-C_2)D^*}=-\phi'(-1), \tag{16}$$

where q'' and m'' represent the local heat and mass fluxes, respectively. It is worth noting that these equations and parameters are specifically tailored to the problem at hand, and their applicability may vary in different mathematical or scientific contexts.

3 Method of the solution

In this section, we apply the SLM to solve the nonlinear system of Eqs (10)–(13) with boundary conditions (14). According to this method, the functions $f(\eta)$, $g(\eta)$, $\theta(\eta)$, and $\phi(\eta)$ are expanded as follows:

$$\left.\begin{aligned} f(\eta) &= f_i(\eta) + \sum_{m=0}^{i-1} F_m(\eta), \\ g(\eta) &= g_i(\eta) + \sum_{m=0}^{i-1} G_m(\eta), \\ \theta(\eta) &= \theta_i(\eta) + \sum_{m=0}^{i-1} \Theta_m(\eta), \\ \phi(\eta) &= \phi_i(\eta) + \sum_{m=0}^{i-1} \Phi_m(\eta), \end{aligned}\right\} \tag{17}$$

where the symbols f_i, g_i, θ_i, and ϕ_i are used to represent the unknown functions, whereas F_m, G_m, Θ_m, and Φ_m ($m = 0, 1, 2, \ldots$) are the successive approximations obtained through iterative solutions of the linear part of the equation system derived by substituting Eq. (17) into Eqs (10)–(13). The fundamental assumption that underlies the SLM is that as the iteration index i increases, the functions f_i, g_i, θ_i, and ϕ_i tend to approach zero. As a result, the nonlinear terms and their derivatives in f_i, g_i, θ_i, and ϕ_i are considered negligible and are disregarded. To start the iterative procedure, initial guesses for $F_0(\eta)$, $G_0(\eta)$, $\Theta_0(\eta)$, and $\Phi_0(\eta)$ were selected to fulfill the specified boundary conditions:

$$\left.\begin{aligned} &\eta = -1 : F = F' = G = 0, \quad \Theta = \Phi = 1, \quad \text{and} \\ &\eta = +1 : F = \Theta = \Phi = 0, \quad F' = -1, G = 1. \end{aligned}\right\}$$

The suitable initial guesses are as follows:

$$F_0(\eta) = (1 + \eta - \eta^2 - \eta^3)/4, \quad G_0(\eta) = (1 + \eta)/2,$$
$$\Theta_0(\eta) = \Phi_0(\eta) = (1 - \eta)/2.$$

The linearized equations that need to be solved are then given by:

$$a_{1,i-1}F_i^{iv} + a_{2,i-1}F'''_i + a_{3,i-1}F_i'' + a_{4,i-1}F_i' + a_{5,i-1}F_i + a_{6,i-1}G_i = r_{1,i-1}, \tag{18}$$

$$b_{1,i-1}F_i'' + b_{2,i-1}F_i' + b_{3,i-1}F_i + b_{4,i-1}G_i'' + b_{5,i-1}G_i' + b_{6,i-1}G_i = r_{2,i-1}, \tag{19}$$

$$c_{1,i-1}F_i' + c_{2,i-1}F_i + c_{3,i-1}\Theta_i'' + c_{4,i-1}\Theta_i' + c_{5,i-1}\Theta_i = r_{3,i-1}, \tag{20}$$

$$d_{1,i-1}F_i' + d_{2,i-1}F_i + d_{3,i-1}\Phi_i'' + d_{4,i-1}\Phi_i' + d_{5,i-1}\Phi_i = r_{4,i-1}, \tag{21}$$

where

$$a_{1,i-1} = 1 + N_1, \quad a_{2,i-1} = -\mathrm{Re}\sum_{m=0}^{i-1} F_m,$$
$$a_{3,i-1} = \mathrm{Re}\sum_{m=0}^{i-1} F_m', \quad a_{4,i-1} = \mathrm{Re}\sum_{m=0}^{i-1} F_m'',$$
$$a_{5,i-1} = -\mathrm{Re}\sum_{m=0}^{i-1} F'''_m, \quad a_{6,i-1} = -N_1, \quad b_{1,i-1} = N_1,$$
$$b_{2,i-1} = N_3\mathrm{Re}\sum_{m=0}^{i-1} G_m,$$
$$b_{3,i-1} = -N_3\mathrm{Re}\sum_{m=0}^{i-1} G_m', \quad b_{4,i-1} = N_2,$$
$$b_{5,i-1} = -N_3\mathrm{Re}\sum_{m=0}^{i-1} F_m, \quad b_{6,i-1} = N_3\mathrm{Re}\sum_{m=0}^{i-1} F_m' - 2N_1,$$
$$c_{1,i-1} = \mathrm{Pe}_h\sum_{m=0}^{i-1} \Theta_m, \quad c_{2,i-1} = -\mathrm{Pe}_h\sum_{m=0}^{i-1} \Theta_m',$$
$$c_{3,i-1} = 1, \quad c_{4,i-1} = -\mathrm{Pe}_h\sum_{m=0}^{i-1} F_m, \quad c_{5,i-1} = \mathrm{Pe}_h\sum_{m=0}^{i-1} F_m',$$
$$d_{1,i-1} = \mathrm{Pe}_m\sum_{m=0}^{i-1} \Phi_m, \quad d_{2,i-1} = -\mathrm{Pe}_m\sum_{m=0}^{i-1} \Phi_m',$$
$$d_{3,i-1} = 1, \quad d_{4,i-1} = -\mathrm{Pe}_m\sum_{m=0}^{i-1} F_m, \quad d_{5,i-1} = \mathrm{Pe}_m\sum_{m=0}^{i-1} F_m',$$
$$r_{1,i-1} = \mathrm{Re}\sum_{m=0}^{i-1} Fm\sum_{m=0}^{i-1} F'''_m - \mathrm{Re}\sum_{m=0}^{i-1} F_m'\sum_{m=0}^{i-1} F_m'' - N_1\sum_{m=0}^{i-1} F_m^{iv} + N1\sum_{m=0}^{i-1} G_m - \sum_{m=0}^{i-1} F_m^{iv},$$
$$r_{2,i-1} = N_3\mathrm{Re}\sum_{m=0}^{i-1} F_m\sum_{m=0}^{i-1} G_m' - N_3\mathrm{Re}\sum_{m=0}^{i-1} F_m'\sum_{m=0}^{i-1} G_m - N_1\sum_{m=0}^{i-1} F_m'' + 2N_1\sum_{m=0}^{i-1} G_m - N_2\sum_{m=0}^{i-1} G_m'',$$
$$r_{3,i-1} = \mathrm{Pe}_h\sum_{m=0}^{i-1} F_m\sum_{m=0}^{i-1} \Theta_m' - \mathrm{Pe}_h\sum_{m=0}^{i-1} F_m' \times \sum_{m=0}^{i-1} \Theta_m - \sum_{m=0}^{i-1} \Theta_m'',$$
$$r_{4,i-1} = \mathrm{Pe}_m\sum_{m=0}^{i-1} F_m\sum_{m=0}^{i-1} \Phi_m' - \mathrm{Pe}_m\sum_{m=0}^{i-1} F_m'\sum_{m=0}^{i-1} \Phi_m - \sum_{m=0}^{i-1} \Phi_m''.$$

The boundary conditions are reduced to:

$$F_i(-1) = F_i'(-1) = F_i(1) = F_i'(1) = G_i(-1) = G_i(1) = \Theta_i(-1) = \Theta_i(1) = \Phi_i(-1) = \Phi_i(1) = 0.$$

By applying an iterative approach, we can solve the linearized Eqs (18)–(21) and then obtain the corresponding solutions F_i, G_i, Θ_i, and Φ_i for $i \geq 1$. Through a series of iterations, the solutions can be refined and improved. After performing a sufficient number of iterations, denoted by M, we arrive at the final solutions for $f(\eta), g(\eta), \theta(\eta)$, and $\phi(\eta)$, which can be expressed as follows:

$$f(\eta) \approx \sum_{m=0}^{M} F_m(\eta), \quad g(\eta) \approx \sum_{m=0}^{M} G_m(\eta),$$
$$\theta(\eta) \approx \sum_{m=0}^{M} G_m(\eta), \quad \text{and} \quad \phi(\eta) \approx \sum_{m=0}^{M} G_m(\eta).$$

The Chebyshev spectral collocation method [45] was used to solve Eqs (18)–(21). The unknown functions were represented by Chebyshev interpolating polynomials, which were collocated at Gauss–Lobatto points defined by:

$$x_j = \cos\frac{\pi j}{N}, \quad j = 0, 1, 2, \ldots, N, \tag{22}$$

where N is the number of collocation points used. We approximate the functions F_i, G_i, Θ_i, and Φ_i at the points as follows:

$$F_i(x) \approx \sum_{k=0}^{N} F_i(x_k) T_k(x_j),$$
$$G_i(x) \approx \sum_{k=0}^{N} G_i(x_k) T_k(x_j),$$
$$\Theta_i(x) \approx \sum_{k=0}^{N} \Theta_i(x_k) T_k(x_j),$$
$$\Phi_i(x) \approx \sum_{k=0}^{N} \Phi_i(x_k) T_k(x_j), \ j = 0, 1, \ldots, N,$$

Table 2: Impact of Pe_h on $-\theta'(-1)$ and Pe_m on $-\phi'(-1)$, while keeping $N_1 = N_2 = N_3 = \mathrm{Re} = 1$, and $\mathrm{Pe}_m = 0.5$ constant

Pe_h	$-\theta'(-1)$	Pe_m	$-\phi'(-1)$
0.00	0.500000	0.00	0.500000
0.25	0.449865	0.25	0.449865
0.50	0.397547	0.50	0.397547
0.75	0.342897	0.75	0.342897
1.00	0.285753	1.00	0.285752
2.00	0.028455	2.00	0.028055
3.00	−0.286335	3.00	−0.286211
4.00	−0.680103	4.00	−0.676835
5.00	−1.185915	5.00	−1.180452

where T_k is the kth Chebyshev polynomial and is defined by:

$$T_k(x) = \cos[k \cos^{-1}(x)]. \tag{23}$$

Moreover, we express the derivatives of the variables at the collocation points as follows:

$$\frac{\mathrm{d}^r F_i}{\mathrm{d}\eta^r} = \sum_{k=0}^{N} \mathcal{D}_{kj}^r F_i(x_k),$$
$$\frac{\mathrm{d}^r G_i}{\mathrm{d}\eta^r} = \sum_{k=0}^{N} \mathcal{D}_{kj}^r G_i(x_k),$$
$$\frac{\mathrm{d}^r \Theta_i}{\mathrm{d}\eta^r} = \sum_{k=0}^{N} \mathcal{D}_{kj}^r \Theta_i(x_k),$$
$$\frac{\mathrm{d}^r \Phi_i}{\mathrm{d}\eta^r} = \sum_{k=0}^{N} \mathcal{D}_{kj}^r \Phi_i(x_k), \tag{24}$$

where, $j = 0, 1, \ldots, N, r$ is the order of differentiation, and $\mathcal{D}$ is the Chebyshev spectral differentiation matrix [46]. By inserting Eqs (22)–(24) into Eqs (18)–(21), we obtain the matrix equation:

$$\mathbf{A}_{i-1}\mathbf{X}_i = \mathbf{R}_{i-1}, \tag{25}$$

Table 1: Comparative analysis of the AGM [33], numerical results [33], and SLM for the concentration profile $\phi(\eta)$ at various Reynolds numbers (Re) and Peclet numbers Pe_m, under the conditions of $\mathrm{Pe}_h = 0.2$ and $N_1 = N_2 = N_3 = 0.1$

η	$\mathrm{Re} = 1, \mathrm{Pe}_m = 0.5$			$\mathrm{Re} = 0.5, \mathrm{Pe}_m = 0.25$		
	AGM [33]	NUM [33]	SLM	AGM [33]	NUM [33]	SLM
−1	1	1	1	1	1	1
−0.8	0.9193811169	0.9192939269	0.9192939277	0.9077206890	0.9077116680	0.9077116679
−0.6	0.8358088531	0.8356460368	0.8356460383	0.8142270240	0.8142102267	0.8142102266
−0.4	0.7473962040	0.7471790040	0.7471790058	0.7187645630	0.7187421955	0.7187421955
−0.2	0.6532642196	0.6530205940	0.6530205958	0.6210051590	0.6209800569	0.6209800570
0	0.5533690723	0.5531286373	0.5531286389	0.5209633680	0.5209385166	0.5209385167
0.2	0.4483206457	0.4481088763	0.4481088776	0.4189111730	0.4188891701	0.4188891702
0.4	0.3391859739	0.3390200357	0.3390200367	0.3152899270	0.3152725867	0.3152725868
0.6	0.2272708614	0.2271589176	0.2271589183	0.2106184420	0.2106066932	0.2106066932
0.8	0.1138730124	0.1138170680	0.1138170683	0.1053961140	0.1053902317	0.1053902317
1	0	0	0	0	0	0

where $\mathbf{A}i-1$ is a $(4N+4)\times(4N+4)$ square matrix, and $\mathbf{X}i$ and $\mathbf{R}i-1$ are $(4N+4)\times 1$ column vectors and are defined by:

$$\mathbf{A}_{i-1}=\begin{bmatrix} A_{11} & A_{12} & \mathbf{0} & \mathbf{0} \\ A_{21} & A_{22} & \mathbf{0} & \mathbf{0} \\ A_{31} & \mathbf{0} & A_{33} & \mathbf{0} \\ A_{41} & \mathbf{0} & \mathbf{0} & A_{44} \end{bmatrix},$$
$$\mathbf{X}_i=\begin{bmatrix} F_i \\ G_i \\ \Theta_i \\ \Phi_i \end{bmatrix}, \quad \text{and} \quad \mathbf{R}_{i-1}=\begin{bmatrix} \mathbf{r}_{1,i-1} \\ \mathbf{r}_{2,i-1} \\ \mathbf{r}_{3,i-1} \\ \mathbf{r}_{4,i-1} \end{bmatrix}, \tag{26}$$

where

$$F_i=[f_i(x_0), f_i(x_1), \ldots, f_i(x_N)]^T,$$
$$G_i=[g_i(x_0), g_i(x_1), \ldots, g_i(x_N)]^T,$$
$$\Theta_i=[\theta_i(x_0), \theta_i(x_1), \ldots, \theta_i(x_N)]^T,$$
$$\Phi_i=[\phi_i(x_0), \phi_i(x_1), \ldots, \phi_i(x_N)]^T,$$
$$\mathbf{r}_{1,i-1}=[r_{1,i-1}(x_0), r_{1,i-1}(x_1), \ldots, r_{1,i-1}(x_N)]^T,$$
$$\mathbf{r}_{2,i-1}=[r_{2,i-1}(x_0), r_{2,i-1}(x_1), \ldots, r_{2,i-1}(x_N)]^T,$$
$$\mathbf{r}_{3,i-1}=[r_{3,i-1}(x_0), r_{3,i-1}(x_1), \ldots, r_{3,i-1}(x_N)]^T,$$
$$\mathbf{r}_{4,i-1}=[r_{4,i-1}(x_0), r_{4,i-1}(x_1), \ldots, r_{4,i-1}(x_N)]^T,$$
$$A_{11}=\mathbf{a}_{1,i-1}\mathcal{D}^4+\mathbf{a}_{2,i-1}\mathcal{D}^3+\mathbf{a}_{3,i-1}\mathcal{D}^2+\mathbf{a}_{4,i-1}\mathcal{D}+\mathbf{a}_{5,i-1}\mathbf{I},$$
$$A_{12}=\mathbf{a}_{6,i-1}\mathbf{I},$$
$$A_{21}=\mathbf{b}_{1,i-1}\mathcal{D}^2+\mathbf{b}_{2,i-1}\mathcal{D}+\mathbf{b}_{3,i-1}\mathbf{I},$$
$$A_{22}=\mathbf{b}_{4,i-1}\mathcal{D}^2+\mathbf{b}_{5,i-1}\mathcal{D}+\mathbf{b}_{6,i-1}\mathbf{I},$$
$$A_{31}=\mathbf{c}_{1,i-1}\mathcal{D}+\mathbf{c}_{2,i-1}\mathbf{I},$$
$$A_{33}=\mathbf{c}_{3,i-1}\mathcal{D}^2+\mathbf{c}_{4,i-1}\mathcal{D}+\mathbf{c}_{5,i-1}\mathbf{I},$$
$$A_{41}=\mathbf{d}_{1,i-1}\mathcal{D}+\mathbf{d}_{2,i-1}\mathbf{I},$$
$$A_{44}=\mathbf{d}_{3,i-1}\mathcal{D}^2+\mathbf{d}_{4,i-1}\mathcal{D}+\mathbf{d}_{5,i-1}\mathbf{I},$$

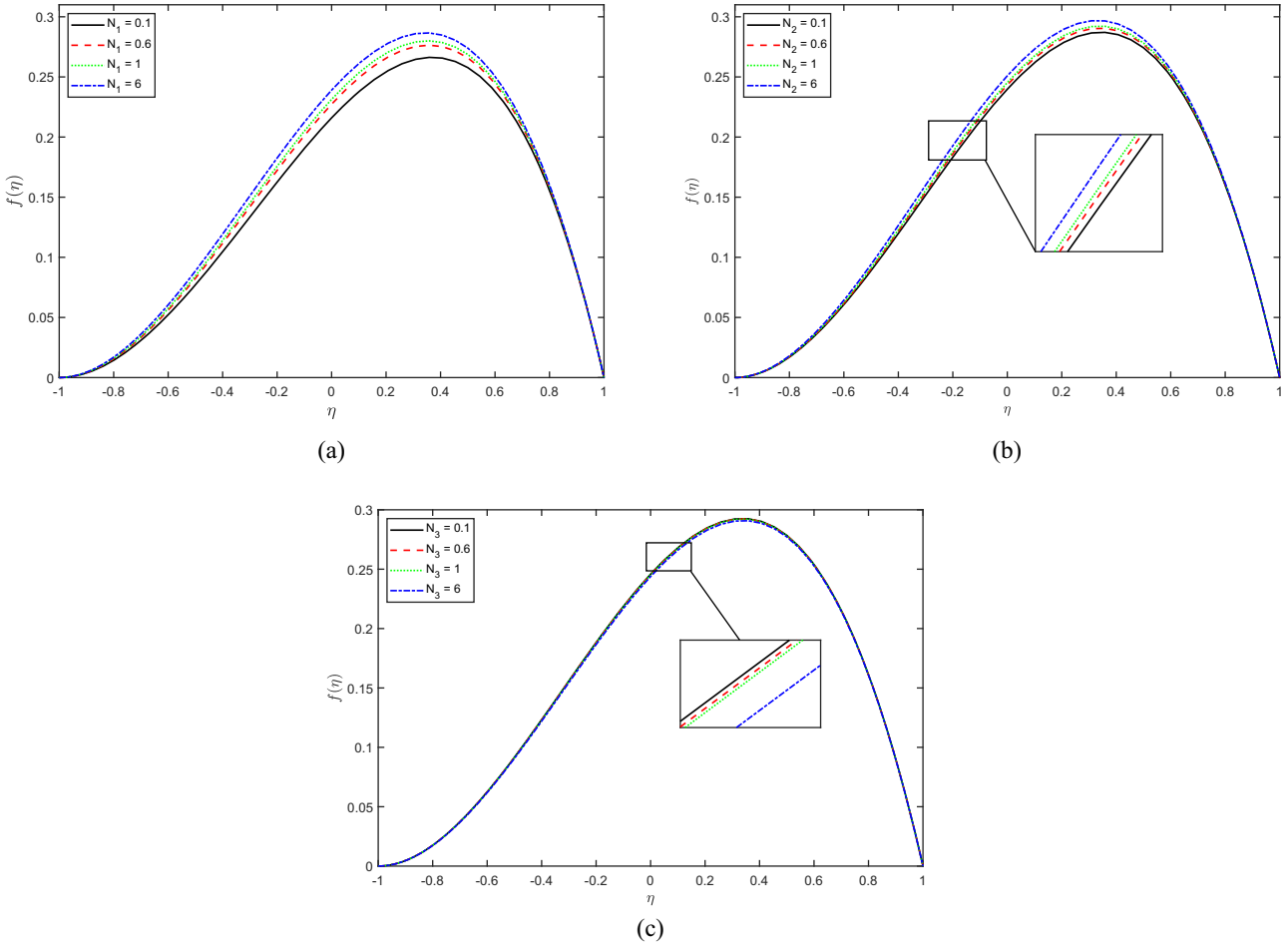

Figure 2: Analysis of the influence of N_1, N_2, and N_3 on the stream function under different conditions: (a) $N_2 = N_3 = 1$, Re = 3, $\mathrm{Pe}_h = 0.2$, and $\mathrm{Pe}_m = 0.5$; (b) $N_2 = N_3 = \mathrm{Re} = 1$, $\mathrm{Pe}_h = 0.2$, and $\mathrm{Pe}_m = 0.5$; and (c) $N_1 = N_2 = \mathrm{Re} = 1$, $\mathrm{Pe}_h = 0.2$, and $\mathrm{Pe}_m = 0.5$.

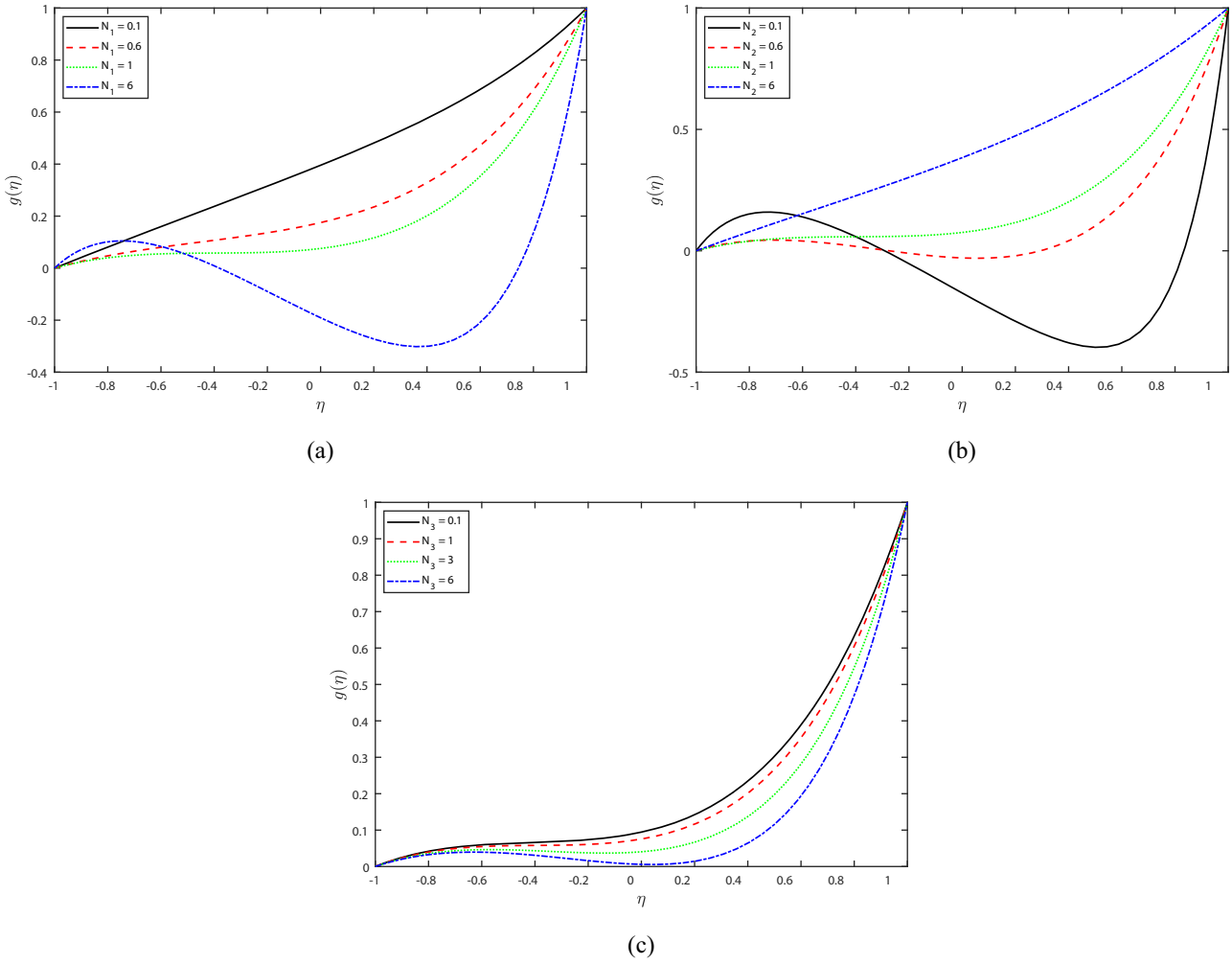

Figure 3: Analysis of the influence of the microrotation profile under different conditions: (a) $N_2 = N_3 = \mathrm{Re} = 1$, $\mathrm{Pe}_h = 0.2$, and $\mathrm{Pe}_m = 0.5$; (b) $N_2 = N_3 = \mathrm{Re} = 1$, $\mathrm{Pe}_h = 0.2$, and $\mathrm{Pe}_m = 0.5$, and (c) $N_1 = N_2 = \mathrm{Re} = 1$, $\mathrm{Pe}_h = 0.2$, and $\mathrm{Pe}_m = 0.5$.

where the symbol T indicates the transposition operation. The matrices $\mathbf{a}_{k,i-1}$, $\mathbf{b}_{k,i-1}$, $(k = 1, \ldots, 6)$, $\mathbf{c}_{j,i-1}$, $\mathbf{d}_{j,i-1}$ $(j = 1, \ldots, 5)$, and $\mathbf{r}_{n,i-1}$, $(n = 1, \ldots, 4)$ are $(N + 1) \times (N + 1)$ diagonal matrices. Matrix $\mathbf{I}$ denotes the identity matrix of size $(N + 1) \times (N + 1)$, and $\mathbf{0}$ represents the zero matrix of size $(N + 1) \times (N + 1)$. Finally, the solution of matrix Eq. (25) is obtained using the inverse of $\mathbf{A}_{i-1}$ as follows:

$$\mathbf{X}_i = \mathbf{A}_{i-1}^{-1}\mathbf{R}_{i-1}. \tag{27}$$

4 Results and discussion

In this section, the solution of the system of nonlinear differential Eqs (10)–(13) with boundary conditions (14) is examined. To obtain the results presented in this study, we applied SLM. On the basis of numerical experiments, we found that $N = 60$ collocation points provide sufficient accuracy for implementing SLM. Through comparative analysis, we established the accuracy and efficiency of our numerical and graphical solutions by comparing them with the results presented by Mirgolbabaee *et al.* [33].

Table 1 provides a comprehensive comparison between the results of applying the SLM technique and those of applying AGM and the Mirgolbabaee numerical method [33]. This table shows excellent agreement between the SLM and numerical results, further confirming the accuracy of the SLM approach.

Table 2 illustrates the influence of the Peclet number on the Nusselt and Sherwood numbers. It is observed that an increase in the Peclet number decreases the Nusselt and Sherwood numbers. This behavior can be attributed to the reduction of momentum transport within the boundary layer with increasing Peclet number.

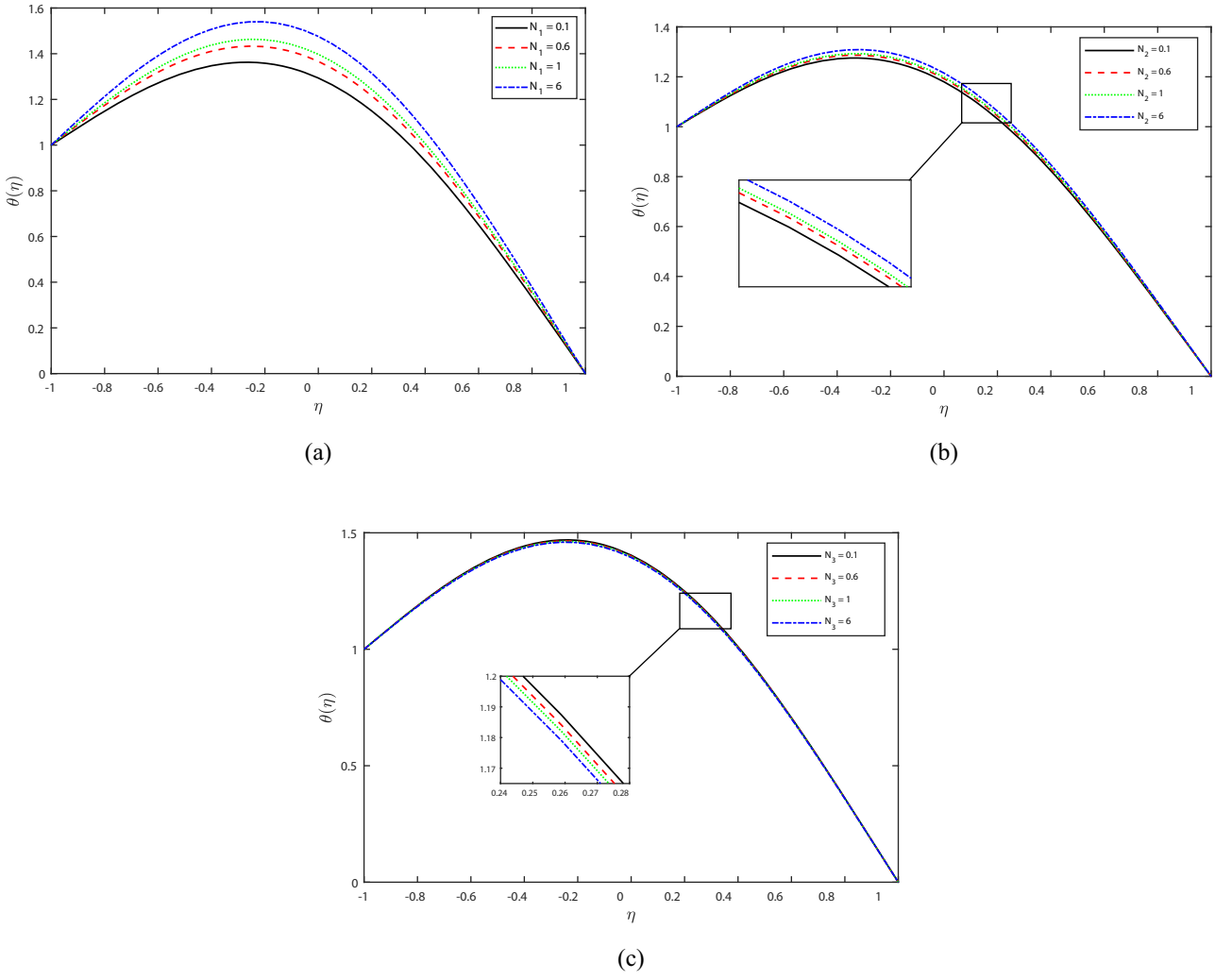

Figure 4: Analysis of the influence of N_1, N_2, and N_3 on the temperature profile under different conditions: (a) $N_2 = N_3 = 1$ and $\mathrm{Pe}_h = \mathrm{Pe}_m = \mathrm{Re} = 5$; (b) $N_1 = N_3 = \mathrm{Re} = 1$, $\mathrm{Pe}_h = 4$, $\mathrm{Pe}_m = 0.5$; and (c) $N_1 = N_2 = 1$ and $\mathrm{Pe}_h = \mathrm{Pe}_m = \mathrm{Re} = 5$.

The influence of different coupling parameters N_1, spin-gradient parameters N_2, and micro-inertia density parameters N_3 on the dimensionless stream function $f(\eta)$, microrotation $g(\eta)$, temperature $\theta(\eta)$, and concentration $\phi(\eta)$ was analyzed in Figures 2–5. Figure 2 shows that the stream function $f(\eta)$ increases with increasing value of N_1 and N_2, while it decreases with increasing value of N_3. Comparable patterns in the temperature and concentration profiles are shown in Figures 4 and 5, respectively. In contrast, as shown in Figure 3, the microrotation profiles $g(\eta)$ generally decrease as N_1 and N_3 grow, but increase as N_2 increases. However, Figure 3(a) shows that the angular velocity at the lower channel wall exhibits oscillatory and irregular behavior when $\eta < -0.5$. Furthermore, Figure 3(b) shows that the angular velocity at the lower channel wall exhibits oscillatory and irregular behavior when $\eta < -0.3$.

The effects of Reynolds number Re on the dimensionless stream function $f(\eta)$, microrotation $g(\eta)$, temperature $\theta(\eta)$, and concentration $\phi(\eta)$ are visually shown in Figure 6. It can be predicted that as the Reynolds number increases, the velocity profile decreases. The Reynolds number can be used to calculate the viscosity of the fluid system, which plays a crucial role in determining the flow pattern. Consistent with physical principles, as the fluid flow rate decreases, the velocity also decreases, and a similar trend is observed in the microrotation, temperature, and concentration profiles.

In Figure 7(a), we can see that as the Peclet number Pe_h increases, the temperature of the liquid $\theta(\eta)$ also increases. This is because momentum diffusivity and inertial forces have a greater influence on the temperature profile. Similarly, in Figure 7(b), we observe the effect of the Peclet number Pe_m on the concentration profile $\phi(\eta)$. An increase

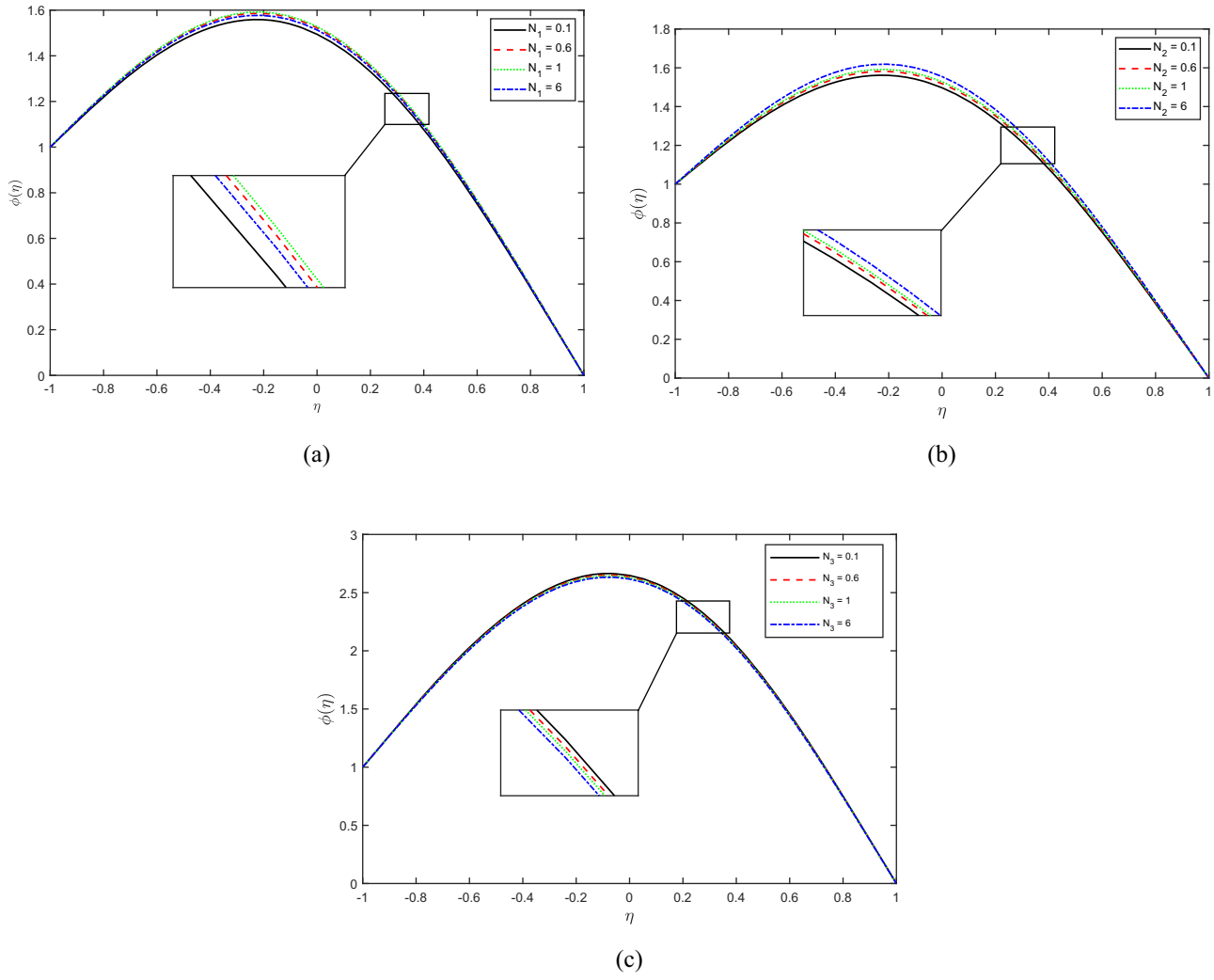

Figure 5: Analysis of the influence of N_1, N_2, and N_3 on the concentration profile under different conditions: (a) $N_2 = N_3 = \text{Re} = 1$, $\text{Pe}_h = 2$, and $\text{Pe}_m = 5$; (b) $N_1 = N_3 = \text{Re} = 1$, $\text{Pe}_h = 2$, and $\text{Pe}_m = 5$; and (c) $N_1 = N_2 = 1$, $\text{Pe}_h = 2.5$, $\text{Pe}_m = 7.5$, and $\text{Re} = 5$.

in Pe_m leads to a higher concentration profile $\phi(\eta)$. At $\text{Pe}_m \gg 1$, we can see a concentration peak due to the increased inertial force. In terms of physical properties, Pe is a dimensionless number that indicates the importance of diffusion and advection for a fluid. At $\text{Pe} \ll 1$, diffusive transport dominates, leading to gradual temperature and concentration gradients, slower heat and mass transport, and more uniform distributions. Conversely, for $\text{Pe} \gg 1$, convective transport causes more heterogeneous distributions, faster heat and mass transfer, and steeper temperature and concentration gradients. However, Pe does not play a crucial role in the velocity and microrotation profiles and is not reported in this work.

5 Conclusion

This article presents a numerical study of micropolar fluid flow and heat transfer within a permeable channel. The problem is simplified using similarity variables and solved using the SLM. The results are compared with published results in the study of Mirgolbabaee *et al.* [33] and show excellent agreement. The SLM is a simple but effective method for solving nonlinear boundary value problems. It has high solution convergence, good accuracy, and computing efficiency. This method outperforms classical methods such as R–K, finite difference, finite element, and Keller box methods. It can be extended and applied to other related

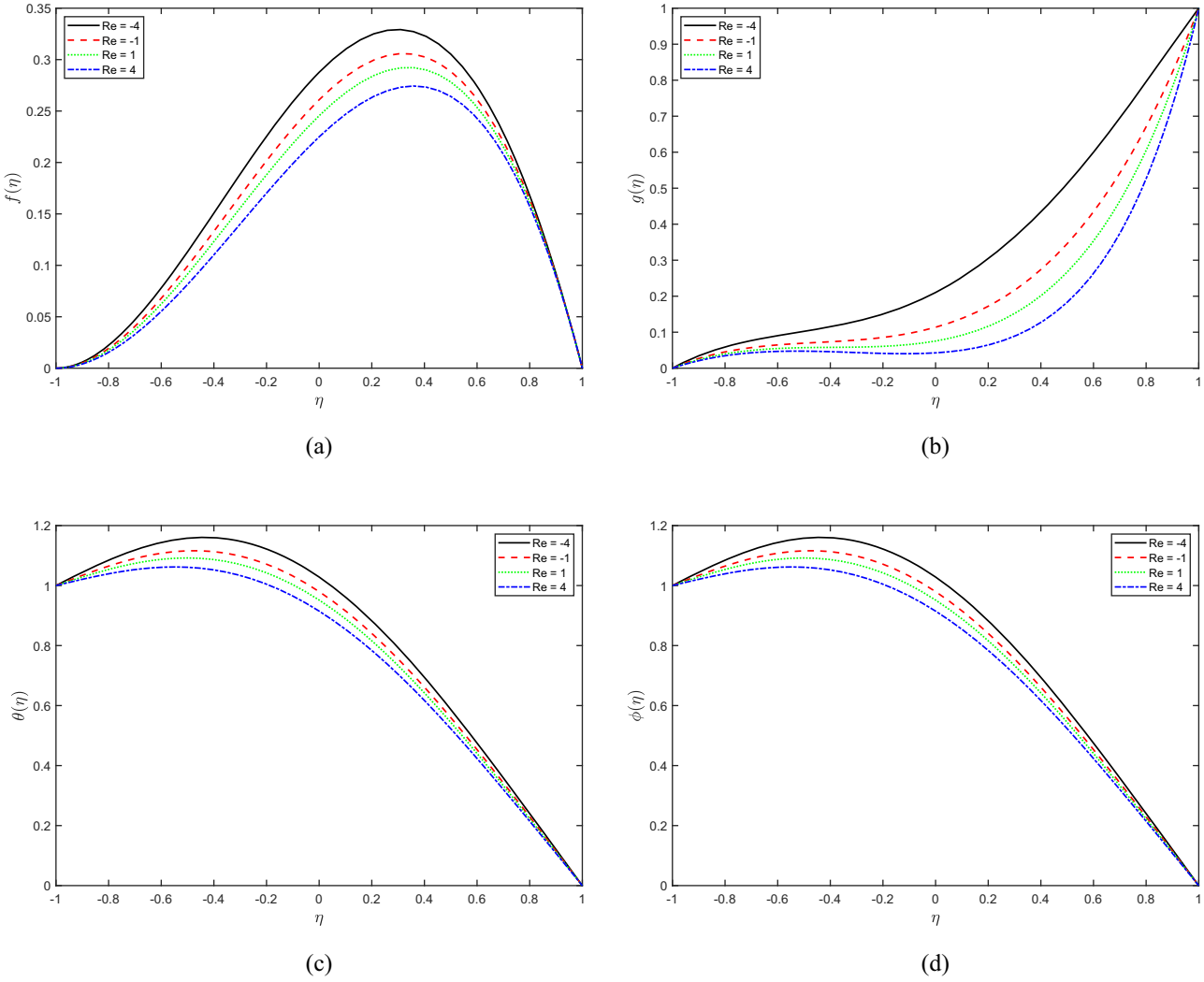

Figure 6: Influence of Reynolds number Re on (a) stream function $f(\eta)$, (b) microrotation $g(\eta)$, (c) temperature $\theta(\eta)$ and (d) concentration $\phi(\eta)$ under the conditions $N_1 = N_2 = N_3 = 1$, $\mathrm{Pe}_h = 0.2$, and $\mathrm{Pe}_m = 0.5$.

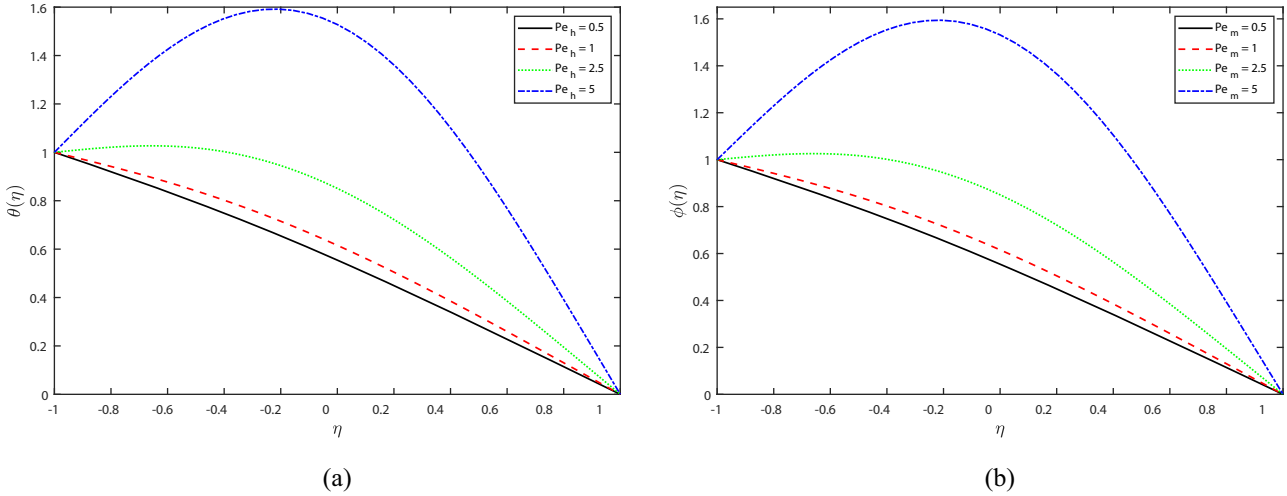

Figure 7: (a) Investigation of the impact of Pe_h on the distribution of temperature under the conditions $N_1 = N_2 = N_3 = \mathrm{Pe}_m = \mathrm{Re} = 1$ and (b) investigation of the influence of Pe_m on concentration under the conditions $N_1 = N_2 = N_3 = \mathrm{Pe}_h = \mathrm{Re} = 1$.

nonlinear boundary value problems of fluid flow models. Key findings from this research include the following:

- Increasing the coupling parameter leads to an improvement in fluid flow, heat transfer, and mass transfer, as indicated by the increased dimensionless stream functions, temperature, and concentration profiles.
- Increase the spin-gradient viscosity parameter and enhance fluid flow, microrotation, heat transfer, and mass transport, as evidenced by the increased dimensionless stream function, microrotation, temperature, and concentration profiles.
- An increase in the micro-inertia density parameter decreases fluid flow, microrotation, heat transfer, and mass transport, which is reflected in the reduction in the dimensionless flow function, microrotation, temperature, and concentration profiles.
- An increase in the Reynolds number decreases the velocity, microrotation, temperature, and concentration profiles. The observed trends in the stream function, temperature, and concentration profiles indicate reduced fluid flow intensity, weaker heat transfer, and reduced mass transport within the system.
- Higher Peclet numbers (Pe_h) correspond to increased fluid temperature, indicating enhanced thermal convection and heat transfer. Likewise, higher Peclet numbers (Pe_m) lead to higher concentration profiles, indicating more efficient mass transport and diffusion processes.
- An increase in the Peclet number decreases the Nusselt and Sherwood numbers, which is due to reduced momentum transport within the boundary layer.

Acknowledgments: The author appreciates the reviewers' valuable comments, which substantially enhanced the manuscript's readability and quality.

Funding information: The author expresses gratitude to the Deanship of Scientific Research at Taif University, Saudi Arabia, for their financial support.

Author contributions: The author has accepted responsibility for the entire content of this manuscript and approved its submission.

Conflict of interest: The author states no conflict of interest.

References

[1] Eringen AC. Theory of micropolar fluids. J Math Mech. 1966;16:1–18.
[2] Gorla RSR, Pender R, Eppich J. Heat transfer in micropolar boundary layer flow over a flat plate. Int J Eng Sci. 1983;21(7):791–8.
[3] Gorla RSR. Buoyancy effects on the boundary layer flow of a micropolar fluid along a vertical cylinder. Int J Eng Sci. 1988;26(8):883–92.
[4] Gorla RSR. Mixed convection in a micropolar fluid from a vertical surface with uniform heat flux. Int J Eng Sci 1992;30(3):349–58.
[5] Arafa AA, Gorla RSR. Mixed convection boundary layer flow of a micropolar fluid along vertical cylinders and needles. Int J Eng Sci. 1992;30(12):1745–51.
[6] Raptis A. Boundary layer flow of a micropolar fluid through a porous medium. J Porous Media. 2000;3(1):95–7.
[7] Ziabakhsh Z, Domairry G. Homotopy analysis solution of micropolar flow in a porous channel with high mass transfer. Adv Theor Appl Mech. 2008;1(2):79–94.
[8] Mohamed RA, Abo-Dahab SM. Influence of chemical reaction and thermal radiation on the heat and mass transfer in MHD micropolar flow over a vertical moving porous plate in a porous medium with heat generation. Int J Therm Sci. 2009;48(9):1800–13.
[9] Rashidi MM, Keimanesh M, Bég OA, Hung TK. Magnetohydrodynamic biorheological transport phenomena in a porous medium: a simulation of magnetic blood flow control and filtration. Int J Numer Meth Biomed Eng. 2011;27(6):805–21.
[10] Turkyilmazoglu M. A note on micropolar fluid flow and heat transfer over a porous shrinking sheet. Int J Heat Mass Transfer. 2014;72:388–91.
[11] Prakash D, Muthtamilselvan M. Effect of radiation on transient MHD flow of micropolar fluid between porous vertical channel with boundary conditions of the third kind. Ain Shams Eng J. 2014;5(4):1277–86.
[12] Fakour M, Vahabzadeh A, Ganji DD, Hatami M. Analytical study of micropolar fluid flow and heat transfer in a channel with permeable walls. J Mol Liq. 2015;204:198–204.
[13] Turkyilmazoglu M. Flow of a micropolar fluid due to a porous stretching sheet and heat transfer. Int J Non-Linear Mech. 2016;83:59–64.
[14] Sheikholeslami M, Ganji DD, Rashidi MM. Magnetic field effect on unsteady nanofluid flow and heat transfer using Buongiorno model. J Magn Magn Mater. 2016;416:164–73.
[15] Sheikholeslami M, Rashidi MM, Hayat T, Ganji DD. Free convection of magnetic nanofluid considering MFD viscosity effect. J Mol Liq. 2016;218:393–9.
[16] Mirzaaghaian A, Ganji DD. Application of differential transformation method in micropolar fluid flow and heat transfer through permeable walls. Alexandria Eng J. 2016;55(3):2183–91.
[17] Doh DH, Muthtamilselvan M, Prakash D. Transient heat and mass transfer of micropolar fluid between porous vertical channel with boundary conditions of third kind. Int J Nonlinear SciNumer Simul. 2016;17(5):231–42.
[18] Doh DH, Muthtamilselvan M, Prakash D. Effect of heat generation on transient flow of micropolar fluid in a porous vertical channel. Thermophys Aeromech. 2017;24(2):275–84.
[19] Mishra SR, Hoque MM, Mohanty B, Anika NN. Heat transfer effect on MHD flow of a micropolar fluid through porous medium with uniform heat source and radiation. Nonlinear Eng. 2019;8(1):65–73.
[20] Pattnaik PK, Moapatra DK, Mishra SR. Influence of velocity slip on the MHD flow of a micropolar fluid over a stretching surface. In: Mishra SR, Dhamala TN, Makinde OD, editors. Recent Trends in Applied Mathematics: Select Proceedings of AMSE 2019. Singapore: Springer; 2021. p. 307–321.

[21] Mishra S, Mahanthesh B, Mackolil J, Pattnaik PK. Nonlinear radiation and cross-diffusion effects on the micropolar nanoliquid flow past a stretching sheet with an exponential heat source. Heat Transfer. 2021;50(4):3530–46.
[22] Saraswathy M, Prakash D, Muthtamilselvan M, Al Mdallal QM. Arrhenius energy on asymmetric flow and heat transfer of micropolar fluids with variable properties: A sensitivity approach. Alexandria Eng J. 2022;61(12):12329–52.
[23] Nadeem A, Rehman KU, Wasfi S, Al-Eid A. Theoretical study of non-Newtonian micropolar nanofluid flow over an exponentially stretching surface with free stream velocity. Adv. Mech Eng. 2022;14(7):16878132221107790.
[24] Abbas N, Shatanawi W. Heat and mass transfer of micropolar-Casson nanofluid over vertical variable stretching Riga sheet. Energies. 2022;15(14):4945.
[25] Saraswathy M, Prakash D, Muthtamilselvan M, Al-Mdallal QM. Theoretical study on bio-convection of micropolar fluid with an exploration of Cattaneo-Christov heat flux theory. Int J Mod Phys B. 2023:2450016.
[26] Saraswathy M, Prakash D, Durgaprasad P. MHD micropolar fluid in a porous channel provoked by viscous dissipation and non-linear thermal radiation: an analytical approach. Mathematics. 2023;11(1):183.
[27] Humane PP, Patil VS, Patil AB, Shamshuddin MD. Buongiorno modelled nanoliquid consequence of thermal and solutal convection on the Magneto-micropolar fluid inside an inclined porous stretching device. J Nanofluids. 2023;12(1):211–22.
[28] Shamshuddin MD, Mabood F, Khan WA, Rajput GR. Exploration of thermal Péclet number, vortex viscosity, and Reynolds number on two-dimensional flow of micropolar fluid through a channel due to mixed convection. Heat Transfer. 2023;52(1):854–73.
[29] Shamshuddin MD, Agbaje TM, Asogwa KK, Makanda G, Usman. Chebyshev spectral approach to an exponentially space-based heat generating single-phase nanofluid flowing on an elongated sheet with angled magnetic field. Numer Heat Transf B. 2024;85(2):159–76.
[30] Salawu SO, Obalalu AM, Fatunmbi EO, Shamshuddin MD. Elastic deformation of thermal radiative and convective hybrid SWCNT-Ag and MWCNT-MoS4 magneto-nanofluids flow in a cylinder. Results Mater. 2023;17:100380.
[31] Harwin DA. Flows in porous channels [dissertation]. United Kingdom: University of Bath; 2007.
[32] Jalili B, Azar AA, Jalili P, Ganji DD. Analytical approach for micropolar fluid flow in a channel with porous walls. Alexandria Eng J. 2023;79:196–226.
[33] Mirgolbabaee H, Ledari ST, Ganji DD. Semi-analytical investigation on micropolar fluid flow and heat transfer in a permeable channel using AGM. J Assoc Arab Univ Basic Appl Sci. 2017;24:213–22.
[34] Makukula Z, Sibanda P, Motsa S. A note on the solution of the von Kármán equations using series and Chebyshev spectral methods. Boundary Value Probl. 2010;2010:1–17.
[35] Makukula Z, Sibanda P, Motsa SS. A novel numerical technique for two-dimensional laminar flow between two moving porous walls. Math Probl Eng. 2010;2010:528956.
[36] Shateyi S, Motsa SS. Variable viscosity on magnetohydrodynamic fluid flow and heat transfer over an unsteady stretching surface with Hall effect. Boundary Value Probl. 2010;2010:257568.
[37] Ahmed MAM, Mohammed ME, Khidir AA. The effects of cross-diffusion and radiation on mixed convection from a vertical flat plate embedded in a fluid-saturated porous medium in the presence of viscous dissipation. Propuls Power Res. 2016;5(2):149–63.
[38] Ahmed MAM, Mohammed ME, Khidir AA. On linearization method to MHD boundary layer convective heat transfer with low pressure gradient. Propuls Power Res. 2015;4(2):105–13.
[39] Daoud Y, Abdalbagi M, Khidir AA. On the solution of magneto-hydrodynamics three-dimensional flow due to a stretching sheet in a porous medium using the successive linearization method. Chin J Phys. 2021;73:232–8.
[40] Awad FG, Sibanda P, Motsa SS, Makinde OD. Convection from an inverted cone in a porous medium with cross-diffusion effects. Comput Math Appl. 2011;61(5):1431–41.
[41] Salah F, Alzahrani AK, Sidahmed AO, Viswanathan KK. A note on thin-film flow of Eyring-Powell fluid on the vertically moving belt using successive linearization method. Int J Adv Appl Sci. 2019;6(2):17–22.
[42] Awad FG, Sibanda P, Narayana M, Motsa SS. Convection from a semi-finite plate in a fluid-saturated porous medium with cross-diffusion and radiative heat transfer. Int J Phys Sci. 2011;6(21):4910–23.
[43] Makukula Z, Motsa SS, Sibanda P. On a new solution for the viscoelastic squeezing flow between two parallel plates. J Adv Res Appl Math. 2010;2(4):31–38.
[44] Sibanda P, Awad F. Flow of a micropolar fluid in a channel with heat and mass transfer. In: Proceedings of the 2010 International Conference on Theoretical and Applied Mechanics. International Conference on Fluid Mechanics and Heat and Mass Transfer, Corfu Island, Greece, July 22–24, 2010. p. 112–20.
[45] Canuto C, Hussaini MY, Quarteroni A, Zang TA. Spectral methods in fluid dynamics. Berlin: Springer-Verlag; 1988.
[46] Trefethen LN. Spectral methods in MATLAB. Philadelphia: Society for industrial and applied mathematics; 2000.